

Learning Granularity-Aware Affordances from Human-Object Interaction for Tool-Based Functional Grasping in Dexterous Robotics

Fan Yang, Wenrui Chen, Kailun Yang, Haoran Lin, DongSheng Luo, Conghui Tang, Zhiyong Li, and Yaonan Wang

arXiv:2407.00614v1 [cs.RO] 30 Jun 2024

Abstract—To enable robots to use tools, the initial step is teaching robots to employ dexterous gestures for touching specific areas precisely where tasks are performed. Affordance features of objects serve as a bridge in the functional interaction between agents and objects. However, leveraging these affordance cues to help robots achieve functional tool grasping remains unresolved. To address this, we propose a granularity-aware affordance feature extraction method for locating functional affordance areas and predicting dexterous coarse gestures. We study the intrinsic mechanisms of human tool use. On one hand, we use fine-grained affordance features of object-functional finger contact areas to locate functional affordance regions. On the other hand, we use highly activated coarse-grained affordance features in hand-object interaction regions to predict grasp gestures. Additionally, we introduce a model-based post-processing module that includes functional finger coordinate localization, finger-to-end coordinate transformation, and force feedback-based coarse-to-fine grasping. This forms a complete dexterous robotic functional grasping framework GAAF-Dex, which learns Granularity-Aware Affordances from human-object interaction for tool-based Functional grasping in Dexterous Robotics. Unlike fully-supervised methods that require extensive data annotation, we employ a weakly supervised approach to extract relevant cues from exocentric (Exo) images of hand-object interactions to supervise feature extraction in egocentric (Ego) images. Correspondingly, we have constructed a small-scale dataset, FAH, which includes near 6K images of functional hand-object interaction Exo images and Ego images of 18 commonly used tools performing 6 tasks. Extensive experiments on the dataset demonstrate that our method outperforms state-of-the-art methods, and real-world localization and grasping experiments validate the practical applicability of our approach. The source code and the established dataset will be made publicly available at <https://github.com/yangfan293/GAAF-DEX>.

Index Terms—Visual Affordance, Dexterous Grasping, Dexterous Hand, Tool Manipulation, Hand-Object Interaction.

I. INTRODUCTION

This work was partially supported by the National Key R&D Program of China under Grant 2022YFB4701404, the National Natural Science Foundation of China under Grant 62273137 and U23A201343, Hunan Province R&D project under Grant 2022SK218, the Hunan Science Fund for Distinguished Young Scholars under Grant 2024JJ2027. (Corresponding author: Wenrui Chen.)

F. Yang, W. Chen, K. Yang, H. Lin, D. Luo, and C. Tang are with the School of Robotics, Hunan University, Changsha 410012, China. (e-mail: ysyf293@hnu.edu.cn; chenwenrui@hnu.edu.cn.)

W. Chen, K. Yang, Z. Li, and Y. Wang are also with the National Engineering Research Center of Robot Visual Perception and Control Technology, Hunan University, Changsha 410082, China.

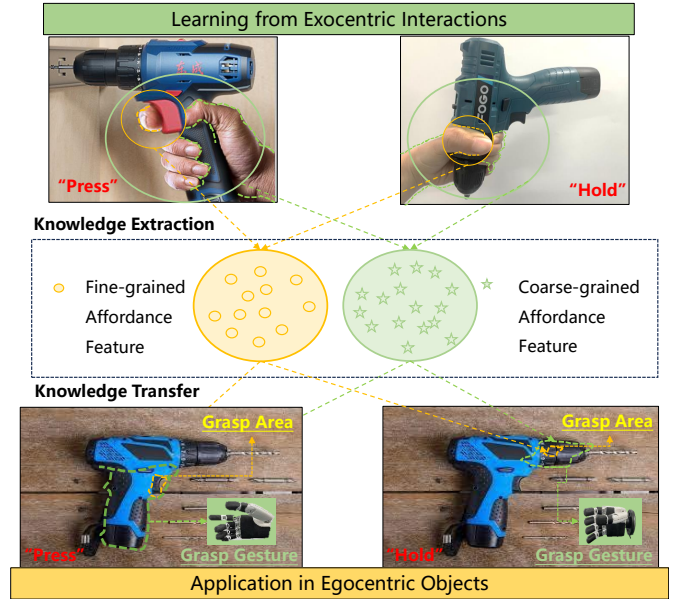


Fig. 1. By extracting knowledge of different granularity from exocentric images (*i.e.*, coarse-grained affordance features related to coarse grasping gestures and fine-grained affordance features related to the grasping regions), we transfer this knowledge to egocentric images of new object instances for functional grasp area localization and coarse gesture prediction.

ENABLING robots to use tools to serve humans, the first step is functional grasping [1], which allows robots to learn task-oriented grasping. Functional grasping introduces two new requirements: (i) functional grasping involves grasping specific areas of the object, which are stricter than general grasping contact areas; (ii) functional grasping must use dexterous hands to generate multi-finger grasps, offering more degrees of freedom. This paper considers how, under visual guidance, we can accomplish functional grasping based on the constraints of the object itself and the task.

In the past, the grasp of vision-based grasp often focused on 6D pose estimation [2]–[4], but they can only estimate the overall position and orientation of objects, which cannot locate the more stringent functional grasping areas, nor can they predict the grasping gestures required for functional grasping. On the other hand, data-driven and reinforcement learning-based approaches have attempted to derive hand-object interaction parameters directly from input images. However, data-driven methods [5]–[9] rely on extensive annotated data to

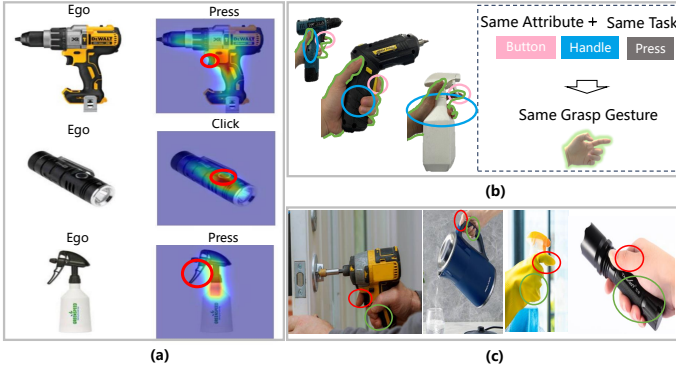


Fig. 2. Illustration of the motivation of our work. (a) Tool function grasp requires more fine-grained affordance grounding, as shown by the red circle. (b) Objects with the same structural attributes in the interaction area typically use the same gestures for the same task. (c) The finger that needs to perform a specific function (red circle) has spatial looseness with the other four fingers (green circle).

directly regress grasping contact points and postures, which is inefficient and non-scalable when annotating hundreds of high-degree-of-freedom grasping poses in real-world settings. Meanwhile, leveraging deep reinforcement learning [8], [10], [11] to train grasping strategies in simulation, which directly outputs the end-effector pose and finger configurations, requires simulation setups and extensive parameter searches to function effectively, often rendering it impractical for real-world applications.

In recent years, the concept of “affordance” [12] has provided new insights for functional grasping. “affordance” provides a bridge between “task” and “action” for functional grasping [13], describing potential physical interactions within object parts, linking object components to operational actions. In the visual understanding field, “object-centered” studies on affordances [14]–[18] are able to detect, segment, and label areas of “action possibilities” on objects. In contrast, “human-centered” studies [19]–[21] can output human postures in response to task commands. After analysis, we find that the structure and attributes of objects themselves contain grasping postures. Objects with the same structural features (e.g., drills and spray bottles both have buttons and handles) typically use the same gestures for the same tasks (e.g., “Press”), as shown in Fig. 2 (b), and this feature is closely related to the hand-object interaction area (affordance). That is, to meet the new demands derived from functional grasping based on the constraints of the object itself and the task, we can utilize the affordance feature of objects.

Based on the discussion above, in this work, we focus on affordance studies for functional grasping, further exploring the derivative problems of functional grasping, providing necessary affordance grounding and coarse grasping gestures for robots, and aiding them in learning to grasp more complex objects, such as tools. To avoid costly data annotation expenses, we refer to more realistic settings [16], [22]–[25], where the task is to learn object visibility through observation of human-object interaction images. Unlike these studies, we not only learn visibility but also dexterous gesture generation. That is, given some interaction images, such as the Exo images

in Fig. 1, along with corresponding labels (e.g., “Press”), the goal is to learn the grasping regions and coarse gestures for new instances of the object. This is a weakly supervised setting where only image-level labels are provided without any pixel-wise annotations.

Existing methods are limited in their ability to fully utilize affordance clues from hand-object interaction images. These limitations manifest in three primary challenges: (i) a focus on isolated tasks of either region localization or gesture prediction without a holistic approach to integrating these tasks; (ii) The affordance grounding works [23], [24] have an inability to precisely identify and utilize regions necessary for functional affordances in complex tasks, as shown by the colored areas in the second column of Fig. 2 (a); (iii) The grasp prediction methods [1], [5], [6] reliance on the MANO [26] hand model which does not translate well to practical applications involving mechanical hands. To effectively address these issues, we propose a comprehensive set of solutions.

First, to bridge the gap between region localization and gesture prediction, we propose a multi-task framework based on affordance feature learning at multiple levels of granularity. This framework extracts multi-level features from interaction regions relevant to the task. Coarse-grained affordance features are utilized for predicting grasping gestures, while fine-grained affordance features are used for predicting grasping regions. This multi-granularity feature extraction allows for a more accurate understanding of how dexterous hands interact with objects during functional tasks, thereby overcoming the limitations of single-task approaches.

Second, addressing the challenge of functional affordance, we define it as the specific regions on an object that functional fingers must contact to execute a task effectively, as shown by the red circles in the second column of Fig. 2 (a). For instance, for the task “Press Drill”, the functional affordance would be the area where the index finger must press. Our solution extends beyond general action area localization to a more refined, functional-finger-guided affordance localization approach. We observe that functional fingers (as shown by the red circles in the second column of Fig. 2 (c)) maintain a spatial distance from other fingers (as indicated by the green circles in the second column of Fig. 2 (c)). Enlightened by this, we leverage spatial analysis and kinematic modeling to calculate the interactions between fingers and the object, enabling us to identify critical contact areas.

Thirdly, to overcome the inadequacies of the MANO [26] hand model for mechanical hands, we design an affordance-driven coarse gesture prediction network tailored for mechanical hands. This network is trained to recognize types of coarse hand gestures commonly used in daily tasks, focusing on features that are most activated during exocentric hand-object interactions. By doing so, the network adapts more effectively to the physical constraints and operational capabilities of actual mechanical hands, improving its utility and applicability in real-world scenarios.

Moreover, to leverage the task consistency of our localization and gesture predictions, we design a model-based post-processing module to effectively combine grasping areas and gestures. Specifically, the keypoint of this module is after

obtaining functional affordance areas and coarse gestures, we use gesture-provided joint angles and a mechanical hand model for coordinate transformation to calculate the transformation matrix from the fingers to the wrist. This enables the arm-hand system to achieve dexterous tool grasping.

Finally, despite advances in visual learning, existing datasets [5]–[7], [27]–[30] still face limitations such as reliance on synthetic data, use of mesh parameters for gestures, and lack of human behavior consideration in affordance area reasoning. To conduct comprehensive research, we propose a foundational dataset for functional affordance understanding named FAH, including nearly 6K images, covering 18 tools across 6 functionalities, along with 14 gesture labels.

In summary, we introduce a multi-task architecture GAAF-Dex, which learns affordance understanding cues for robotic functional grasping from image-based human-object interactions. During inference, it accurately locates fine-grained functional affordance areas in Ego images and generates diverse coarse grasp gestures suitable for different objects and tasks. Our contributions are outlined as follows:

- A multi-task learning framework, GAAF-Dex, is put forward to learn grasping knowledge from the exocentric perspective and transfer it to the egocentric perspective. GAAF-Dex deconstructs affordance features to predict affordance locations and coarse gestures for dexterous functional grasping, followed by a post-processing task.
- A functional-finger-guided fine-grained affordance localization method is designed, which leverages the spatial distribution of fingers in hand-object interaction images to extract finer-grained features for functional affordance localization.
- An affordance-driven mechanical gesture prediction network is developed, using highly activated features in hand-object interaction regions for different tasks and tools to output various gestures, directly applicable to mechanical hands.
- Extensive experiments on the FAH dataset and real-world scenarios demonstrate the effectiveness of our approach. The FAH dataset includes functional hand-tool interaction images in the exocentric perspective, which can be learned and transferred to the egocentric perspective.

II. RELATED WORK

Visual Affordance Understanding. Research in vision-based affordance understanding aims to locate areas of objects that are operable. Various methodologies have inferred visual affordances for simple gripper grasps [13], [18], [31], [32]. Chen *et al.* [33] propose a framework for detecting 6-DoF task-oriented grasps, processing observed object point clouds to predict diverse grasping poses tailored for distinct tasks. The studies [34], [35] are conducted to generalize the robot grasping affordance areas beyond labels by incorporating large prediction models.

In contrast, works such as those in [18], [24], [27] explore non-robot-centric visibility. Early efforts focused on acquiring affordances using fully supervised methods requiring per-pixel labeling, leading to substantial data acquisition costs [27],

TABLE I
STATISTICS OF RELATED DATASETS AND THE PROPOSED FAH DATASET.
INTER-TYPE: INTERACTION TYPE (HA-O: HAND-OBJECT, HU-O: HUMAN-OBJECT).
REAL / SYN.: REAL OR SYNTHETIC DATA. VIEW: PERSPECTIVE. ANNOTATION:
LEVEL OF ANNOTATION (PIX-LEVEL: PIXEL-LEVEL, IMG-LEVEL: IMAGE-LEVEL).
HAND POSE: ANNOTATION TYPE (MESH: HAND MESH, ANGLE: JOINT ANGLES).
AFF. INT.: AFFORDANCE INTERACTION (✓: YES, ×: NO)

Dataset	Year	Inter-Type	Real / Syn.	View	Annotation	Hand Pose	Aff. Int
ObMan [30]	2019	Ha-O	syn.	Exo	Pix-Level	Mesh	×
YCBAfford [5]	2020	Ha-O	syn.	Exo	Pix-Level	Mesh	×
PAD [29]	2021	Hu-O	real	Exo-Ego	Pix-Level	×	✓
AGD20K [25]	2021	Hu-O	real	Exo-Ego	Img-Level	×	✓
OakInk-Image [7]	2022	Ha-O	real	Exo	Pix-Level	Mesh	✓
AffordPose [6]	2023	Ha-O	syn.	Exo	Pix-Level	Mesh	✓
OakInk2 [28]	2024	Ha-O	real	Exo	Pix-Level	Mesh	✓
FAH (Ours)	2024	Ha-O	real	Exo-Ego	Img-Level	Angle	✓

[36], [37]. Diverging from this, recent studies [16], [18], [24] have begun exploring weakly supervised approaches for obtaining affordance information, leveraging perspectives from human-object interactions in images [24] or videos [18] to transfer interaction cues to object-only views for affordance supervision. LOCATE [24] supervises egocentric images by aggregating features from exocentric images into compact prototypes (human, object part, and the background), identifying matching object parts within images. Luo *et al.* [18] harness affordance areas by analyzing hand positions and motions in interaction videos, enabling the supervision of images featuring objects alone. However, tool use necessitates a combination of dexterous manipulation and functional part affordance understanding, so we integrate weakly supervised affordances with the generation of dexterous coarse gestures. Our approach not only learns affordance localization from hand-object interactions but also grasping gestures, laying the groundwork for subsequent tool use.

Coarse-to-Fine Dexterous Grasping. Achieving functional tool manipulation with robotic hands necessitates advanced dexterous grasping, which extends beyond basic two or three-finger grippers to involve multi-finger coordination. Previous approaches to achieving precise grasping have relied on either model-based methods [38]–[41], which require extensive time for object and hand modeling and suffer from poor generalization, or data-driven methods [1], [42]–[46], which are costly due to the need for extensive labeling of contact points and joints. In contrast, the coarse-to-fine approach used in [1], [5], [6] treats the task of predicting dexterous gestures as a classification problem. After obtaining a specific category of grasp type, fine-tuning is performed, simplifying the high-dimensional data prediction task. GanHand [5] utilizes 33 grasp classification types of the MANO model [26] to generate pre-grasp postures, whereas FunctionalGrasp [1] maps these 33 grasp types of MANO models to the ShadowHand robotic hand model to obtain pre-grasp postures. In contrast, we have designed a classification network for 14 gestures of a low-cost robotic hand, leveraging the consistency of the object’s “task-affordance”. These 14 gestures encompass the daily tool operation needs of humans.

Hand-Object Interaction Datasets. The emergence of

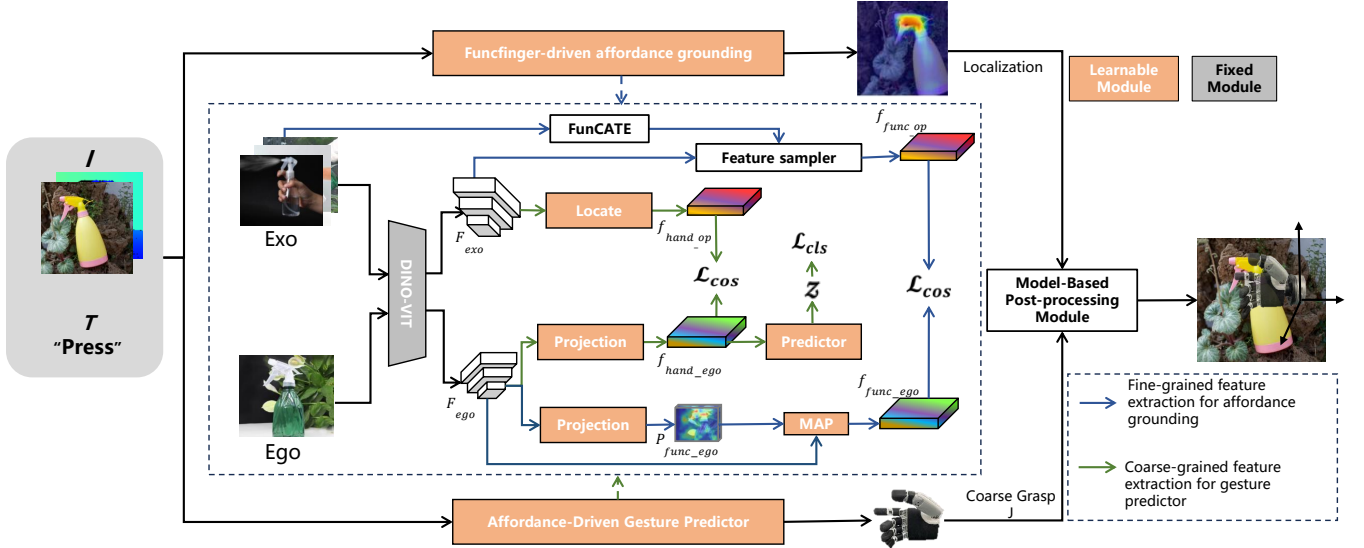


Fig. 3. **Framework of GAAF-Dex.** The outer box with solid arrows represents the inference stage flowchart. Given an RGB-D (The depth map “D” does not participate in training, which only provides the grasping depth directly according to the affordance location) egocentric image and a task as input, the Funcfinger-driven Affordance Grounding (FDAG) module identifies the coordinates of the grasping region, and the Affordance-Driven Gesture Predictor (ADGP) module predicts the corresponding coarse gestures. Finally, the Model-based Post-processing Module integrates and optimizes the coordinates and gestures to achieve the final functional grasp. The inner box with dashed lines illustrates the training flowchart for the FDAG and ADGP modules. Given N exocentric images and one egocentric image as input, both modules are trained using our carefully designed granularity-sensitive affordance feature extraction network. Black arrows represent the common feature extraction process, blue arrows represent the fine-grained affordance feature extraction for localization, and green arrows represent the coarse-grained affordance feature extraction for gesture prediction.

relevant datasets has significantly advanced the development of “hand-object” interactions, as shown in Tab. I. OakInk [7] introduces a dataset containing affordances and corresponding gesture labels for 1800 household objects. AffordPose [6] further introduces a large-scale dataset driven by fine-grained hand-object interactions based on the visibility of specific object parts. However, its datasets are synthetic, and the hand annotations rely heavily on labor-intensive annotations of the MANO model [26], making them less directly applicable to actual dexterous robotic grasping. AGD20K [22] focuses on inferring human intentions from support images of human-object interactions and transferring them to a set of query images. However, it does not consider direct hand-object interactions and lacks gesture annotations. Datasets related to visibility [5]–[7], [27]–[30] face challenges such as reliance on synthetic data, use of mesh parameters for gestures, and failure to consider human behavior in reasoning about affordance areas. We explicitly consider the transition from exocentric to egocentric viewpoints and collect a large number of hand-object interaction images with complete functionality/object categories and part-level annotations, including robotic hand grasp types. These features make our dataset more useful and applicable to real-world scenarios.

III. PROBLEM FORMULATION

The objective of this study is to address challenges in functional grasping by developing a model, denoted by M . This model is designed to analyze egocentric RGB images, I , containing a single object, along with a task description, T . The model outputs the initial grasping area and a coarse

grasping gesture appropriate for the task. Specifically, the model predicts:

$$M(I, T) \rightarrow (P, \{\theta_1, \theta_2, \theta_3, \theta_4, \theta_5\}), \quad (1)$$

where $P=(x, y, z)$ represents the coordinates of the area where the object should be grasped, indicating the initial grasping point within the functional affordance region of the object. The z coordinate is derived from depth maps, providing depth information about the grasping location. The set $\{\theta_1, \theta_2, \theta_3, \theta_4, \theta_5\}$ denotes the joint angles for a coarse grasping gesture. Upon obtaining P and θ_i , a post-processing module refines these predictions to determine the precise hand positions and joint angles required for effective functional grasping.

IV. METHOD

Given a set of exocentric interaction images and an egocentric image of an object, our core objective is to train two prediction modules, namely the Funcfinger-driven affordance grounding and affordance-driven Gesture Predictor modules. They can extract the features of affordance regions related to functional fingers and the corresponding dexterous grasp gestures from the exocentric (Exo) images, and these are then transferred to the egocentric (Ego) image, enabling us to locate the functional finger’s grasp points and gestures within it. During the training phase, we utilize image-level affordance labels, while in the testing phase, the input is an egocentric image, and the outputs are the object’s optimal grasp point P and the associated coarse grasp gesture G , as shown in the external solid line frame in Fig. 3.

The core idea of our method is as follows: for the input images $\{I_{\text{Exo}}, I_{\text{Ego}}\}$ ($I_{\text{Exo}}=\{I_1, I_2, \dots, I_N\}$), we first use a

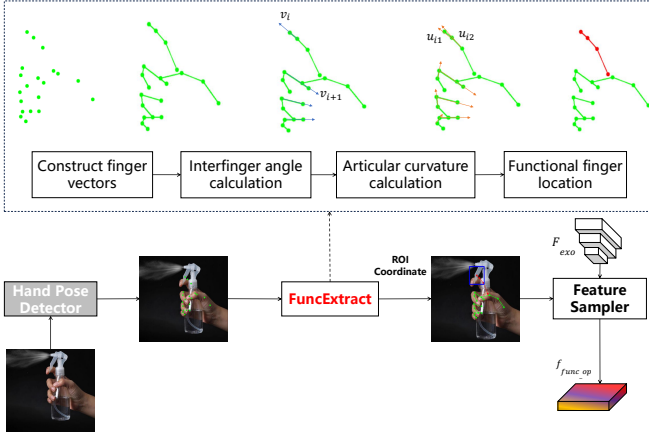


Fig. 4. FunCATE module, which mainly concludes a hand pose detector and FunExtract module. FunExtract mainly determines the functional finger by calculating the vector angles between fingers and the joint angles of each finger. This process identifies the region of interest of the functional finger and extracts the corresponding features.

network ϕ to extract deep features $\{F_{exo}, F_{ego}\} \in \mathbb{R}^{D \times H \times W}$. In our case, ϕ is a self-supervised visual transformer (DINO-ViT [47]), which provides excellent part-level features. Subsequently, depending on different tasks, we process F_{exo} for fine or coarse granularity visibility cue extraction to supervise the corresponding features of F_{ego} for subsequent affordance localization tasks and coarse gesture prediction tasks for functional dexterous grasping. Specifically, for features related to predicting functional areas in Ego images, we propose a Funcfinger-driven method to extract fine-grained functional area features from Exo images for supervision, as detailed in Sec. IV-A. For features related to coarse gesture prediction in Ego images, we refer to the clustering method of the person (hand)-background-object feature prototypes in LOCATE [24]. We obtain coarse-grained features from Exo images to supervise the affordance features used for coarse gesture prediction in Ego images. These coarse-grained features are then used to train the gesture classification network, achieving enhanced gesture prediction based on object features in the hand-object interaction region, as described in Sec. IV-B. Finally, we design a model-based post-processing module to post-process the combination of functional areas and coarse grasp gestures, which results in the final end-effector grasping points and coarse to fine functional grasp, as detailed in Sec. IV-D.

A. Fine-Grained Feature Extraction for Affordance Grounding

As shown by the blue arrows in the dashed box in Fig. 3, we perform fine-grained feature extraction from the previously obtained deep features F_{exo} and F_{ego} to better meet the requirements of functional grasping area localization.

1) *FunCATE*: For feature supervision, we perform functional finger-guided cue extraction on Exo images, primarily implemented by the FunCATE module. Specifically, as shown in Fig. 4, we first use the network ϕ_2 for gesture recognition on Exo images. In our case, ϕ_2 is MediaPipe [48], which has the advantage of accurate landmark detection. It can obtain 21 key points' 3D (x, y, z) coordinates of the human hand.

Then, we apply our proposed functional finger determination algorithm, FuncExtract, which will be detailed in section C, to obtain the 3D (x, y, z) coordinates of the functional fingertip. We consider the area with radius r around these coordinates as our region of interest (ROI) region. Finally, by performing ROI feature extraction on the multi-granularity features F_{mul} , we obtain the final fine-grained affordance features. The ROI feature extraction process is mathematically formulated as follows:

$$F_{\text{upsampled}} = \text{Upsample}(F_{\text{mul-Exo}}) \quad (2)$$

Here, $F_{\text{upsampled}}$ represents the upsampled feature map, obtained by resizing $F_{\text{mul-Exo}}$ to a size of 448×448 .

$$\text{mask}(x, y) = \begin{cases} 1 & \text{if } \sqrt{(x - x_0)^2 + (y - y_0)^2} \leq r \\ 0 & \text{otherwise} \end{cases} \quad (3)$$

Here, the mask function $\text{mask}(x, y)$ defines a circular region centered at (x_0, y_0) with radius r , creating a binary mask.

$$f_{\text{func-op}} = F_{\text{upsampled}} \odot \text{mask} \quad (4)$$

$f_{\text{func-op}}$ is the ROI feature map, resulting from element-wise multiplication of $F_{\text{upsampled}}$ and the binary mask.

2) *FuncExtract*: The FunExtract module is shown in the dotted box at the top of Fig. 4. We use the vector angle between the fingers and the angle between each finger joint to select functional fingers. To be specific, when we obtain coordinates of 21 points on the human hand, we vectorize each finger's points and then compute the angles between each vector to determine if the four vectors, excluding the thumb, are parallel. The parallelism is evaluated using the cosine of the angle between adjacent finger vectors as follows: The cosine of the angle between vectors formed by adjacent finger joints for the i -th finger (excluding the thumb) is calculated as:

$$\text{angle}_i = \frac{v_i \cdot v_{i+1}}{\|v_i\| \|v_{i+1}\|}, \quad i \in \{1, 2, 3, 4\} \quad (5)$$

Here, v_i represents the vector of the i -th finger, excluding the thumb, the \cdot denotes the dot product of the vectors, and the $\| \cdot \|$ denote their magnitudes.

If the cosine value is less than a threshold, the fingers are considered parallel. Otherwise, we compute the remaining four fingers' bending angle which is calculated by the cosine of the angle between vectors formed by adjacent finger joints as follows. We select the one with the minimum bending angle as the functional finger.

$$\begin{aligned} \text{func_ID} &= \underset{i \in \{1, 2, 3, 4\}}{\text{argmin}} \left(1 - \frac{u_{i1} \cdot u_{i2}}{\|u_{i1}\| \|u_{i2}\|} \right) \\ u_{i1} &= p_{i2} - p_{i1} \\ u_{i2} &= p_{i3} - p_{i2} \end{aligned} \quad (6)$$

Here, p_i represents the coordinates of the i -th joint.

3) *Functional Part-Level Knowledge Transfer*: With the assistance of Funcatet, we have identified the prototype features representing the object's functional components. We then utilize these features to supervise the egocentric localization map P_{ego} . Specifically, we first apply the class activation mapping

(CAM) [49] to the ego image to generate a functionally-aware localization map as follows:

$$P_{\text{func-ego}} = P(F_{\text{ego}} + \text{MLP}(F_{\text{ego}})), \quad (7)$$

where MLP represents a feed-forward layer, and P consists of two 3×3 convolutional layers, normalization layers, and non-linear activation functions, followed by a 1×1 class-aware convolution layer. Each map $P_c \in \mathbb{R}^{H \times W}$ represents the network activation for the c -th interaction.

Then, we perform mask average pooling (MAP) between the normalized localization map and the extracted deep features to aggregate them into an embedding as follows:

$$f_{\text{ego}} = \frac{\sum_{u=1, v=1}^{W, H} P_{\text{func-ego}}^{t, u, v} F_{\text{ego}}^{u, v}}{\sum_{i=1}^W \sum_{j=1}^H P_{\text{func-ego}}^{t, u, v}} \in \mathbb{R}^D, \quad (8)$$

where t denotes the ground-truth category.

Finally, we use cosine loss \mathcal{L}_{cos} and concentration loss \mathcal{L}_c to ensure the features are correctly extracted while maintaining coherence as follows:

$$\mathcal{L}_{\text{cos}} = \max(1 - \frac{f_{op} \cdot f_{ego}}{\|f_{op}\| \|f_{ego}\|} - \alpha, 0), \quad (9)$$

$$\mathcal{L}_c = \sum_c \sum_{u, v} \|\langle u, v \rangle - \langle \bar{u}_c, \bar{v}_c \rangle\| \cdot P_{\text{ego}}^{c, u, v} / z_c, \quad (10)$$

$$\bar{u}_c = \sum_{u, v} u \cdot P_{\text{ego}}^{c, u, v} / z_c, \quad \bar{v}_c = \sum_{u, v} v \cdot P_{\text{ego}}^{c, u, v} / z_c, \quad (11)$$

where α is a margin added to compensate for the domain gap as the two embeddings come from different domains. \bar{u}_c and \bar{v}_c represent the center of the c -th localization map along the u and v axes, and $z_c = \sum_{u, v} P_{\text{func-ego}}^{c, u, v}$ is a normalization term. The concentration loss forces the high activation regions of the localization maps to be close to the geometric center.

B. Affordance-Driven Gesture Predictor

As illustrated by the green arrow in the dashed box in Fig. 3, we perform coarse-grained affordance feature extraction on F_{exo} using a method similar to LOCATE [24]. The core of this method involves clustering the object-background-human features within the hand-object interaction region. Then, based on the Intersection Over Union (IOU) values of the similarity map with F_{ego} and the saliency map obtained from the Ego image processed by DINO-VIT [47], we derive the coarse-grained affordance supervision feature prototype $P_{\text{hand-op}}$.

For the Ego image, we use the same processing method and loss function as for $f_{\text{func-ego}}$ to obtain $f_{\text{hand-ego}}$. Next, the output $f_{\text{hand-ego}}$ is fed into the Global Average Pooling (GAP) layer to obtain the classification score z , which is used to calculate the cross-entropy loss \mathcal{L}_f for optimization.

Finally, as discussed in Sec. I, these coarse-grained affordance features originate from the most active regions of hand-object interactions and include affordance-guided coarse gestures. We add a coarse gesture predictor to $f_{\text{hand-ego}}$. Specifically, we use a fully connected MLP classification network on $f_{\text{hand-ego}}$ to predict the grasp type C , classifying it into one of the 14 grasp types that best suit the target object. This network is trained using the cross-entropy loss $\mathcal{L}_{\text{class}}$.

The predicted grasp type C is associated with a representative hand configuration H_C , consisting of the joint angles of the five fingers and the abduction angle of the thumb.

C. Training Supervision

In summary, during the training phase, the total loss consists of the following four parts:

$$\mathcal{L} = \mathcal{L}_{\text{cos}} + \lambda_c \mathcal{L}_c + \mathcal{L}_{\text{class}} + \mathcal{L}_f \quad (12)$$

where λ_c is the weight balancing these four terms, and \mathcal{L}_f represents the cross-entropy loss of the two branches. During testing, only the Ego branch is maintained. With a task label t and an Ego image as input, the network extracts the t -th localization map as the prediction for the functional area.

D. Model-based Post-processing Module

In this module, we first extract the brightest RGB-D pixel in the functional area and convert the pixel to the global coordinate to obtain the coordinate $P_{wf} = [x_{wf}, y_{wf}, z_{wf}]^T$ in the global coordinate system of the functional fingertip.

Then, based on the proportional relationship and joint angles of the robotic hand model's finger joints, we transform the fingertip coordinates P_{wf} to obtain the wrist end coordinates P_{we} in the global coordinate system. Specifically, as shown in Fig. 5 (d), outside the thumb, the other four fingers of the Inspire hand have the same structure, a motor drives the two finger joints to flex and stretch. We take the index finger as an example as shown in Fig. 5 (a), where P_2, P_3 represent the node of the first and second finger joint rotation axes, respectively. P'_i represents the position of the joint node when the drive motor is in the zero position. Here, $P'_1 - P'_2$ is at an δ angle to the X-axis. P''_f represents the hypothetical position of the fingertip if only the second phalanx moves. We establish a hand coordinate system with P_3 as the origin, O . $P_3 - P'_2$ is the positive direction of the x-axis, and the z-axis coincides with the rotation axis of P_3 .

The coordinate $P_{hf} = [x_{hf}, y_{hf}, z_{hf}]^T$ of the fingertip in the hand coordinate system can be obtained as follows:

$$P_{hf} = R(\theta_2) \begin{bmatrix} l_2 \\ 0 \\ 0 \end{bmatrix} + R(\theta_1 + \theta_2 + \delta) \begin{bmatrix} l_1 \\ 0 \\ 0 \end{bmatrix} \quad (13)$$

where the l_1 and l_2 represent the first and second direct lengths respectively. θ_1 and θ_2 come from the linear transformation of the index finger angle of our predicted coarse gestures.

$$R(\theta) = \begin{bmatrix} \cos \theta & -\sin \theta & 0 \\ \sin \theta & \cos \theta & 0 \\ 0 & 0 & 1 \end{bmatrix}.$$

The thumb is driven by a motor for flexion and extension of the three joints, as shown in Fig. 5 (c). The calculation method of the fingertip to the end in flexion and extension is similar to that of the index finger, but the difference is that the thumb also has a lateral swing movement, as shown in Fig. 5 (b).

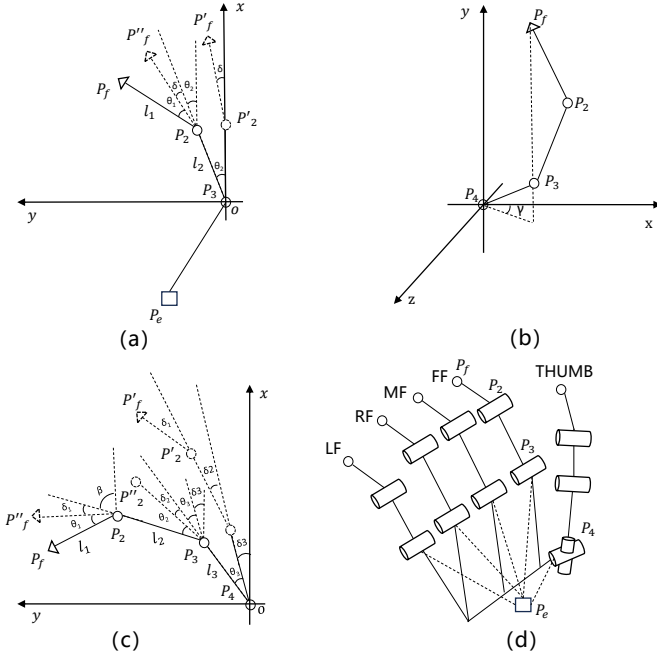


Fig. 5. Diagrams illustrating fingertip-to-end coordinate transformations based on a model. (a) shows the coordinate transformation of the flexion and extension joints of the index finger, (b) shows the coordinate transformation of the abduction and adduction joints of the thumb, (c) shows the coordinate transformation of the flexion and extension joints of the thumb, and (d) provides an overall reference for Inspire hand joints.

The mapping of the fingertip $P_{hf}=[x_{hf}, y_{hf}, z_{hf}]^T$ to the end in the lateral swing process is as follows:

$$P_{hf} = \begin{bmatrix} \cos \gamma & 0 & \sin \gamma \\ 0 & 1 & 0 \\ -\sin \gamma & 0 & \cos \gamma \end{bmatrix} P_{hf}^o \quad (14)$$

where the γ is the abduction-adduction angle, P_{hf}^o is the fingertip coordinates of the thumb in the hand coordinate system calculated from the flexion and extension angle.

The end coordinate P_{we} in the world coordinate system can be obtained by the following equation:

$$P_{we} = R_{wf}(P_{he} - P_{hf}) + P_{wf} \quad (15)$$

where $P_{he}=[x_{he}, y_{he}, z_{he}]^T$ is the wrist end coordinate in the hand coordinate system, which is directly obtained from the mechanical structure. R_{wf} represents the rotation matrix of the object correctly grasped by the hand. Since this method focuses on the functional area and does not involve rotation, we assume that it is a known quantity.

Finally, we adjust the coarse gesture angles, continuously receiving force feedback during the adjustment process. We consider the grasp to be stable and stop the angle adjustment when the rate of change of the force derivative is zero.

V. ESTABLISHED DATASET

To foster research progress in dexterous functional manipulation by enabling robots to learn from human-object interaction examples, we introduce a dataset named FAH for complex dexterous function grasping learning task, which comes from various sources and has rich interactions, and

basically meets the tool use requirements of human in home and industrial scenarios. Specifically, FAH contains a total of nearly 6K images, with 5616 training images, including 3951 Exo images and 1665 Ego images. The test set comprises 242 Ego images. It includes a rich variety of 18 commonly used tools (“Screwdriver”, “Plug”, “Kettle”, “Hammer”, “Spray Bottle”, “Stapler”, “Flashlight”, “Bottle”, “Cup”, “Mouse”, “Knife”, “Pliers”, “Spatula”, “Scissors”, “Door Handle”, “Light Switch”, “Drill”) and 6 tasks (“Press”, “Hold”, “Click”, “Clamp”, “Grip”). Furthermore, we conducted multiple demonstration experiments on these tasks and skills, selecting 14 basic coarse gestures and recording their angle information.

A. Image Collection

Based on those interaction relationships, we meticulously selected corresponding Exo and Ego images from a variety of high-quality sources to ensure a comprehensive dataset. The exocentric images were predominantly sourced from AGD20K [25], detailed tool usage images from e-commerce platforms, and images retrieved using object categories as keywords from freely licensed websites. To address the scarcity of certain interactions online, we enlisted the help of 10 volunteers who photographed themselves using tools according to their natural habits. This effort included detailed interactions with tools like “Clamp Knife”, “Click Kettle”, “Click Mouse”, “Hold Drill”, and “Open Valve”. Our dataset design is particularly notable for its focus on single-hand interaction exocentric images, which are crucial for learning precise functional hand-tool interactions. This choice ensures that the learned features are robust and transferable to egocentric perspectives. Consequently, we filtered out multi-hand images, as they could interfere with the fine-grained affordance feature extraction guided by functional fingers. For the egocentric images, which do not involve human-object interactions, we directly selected standalone tool images from the same rich sources.

B. Data Annotation

Image-level Annotation: We provided image-level labels for the training set, assigning specific affordance and object category labels based on actual human-object interactions. Our task and tool mappings show a many-to-many relationship, with 23 in total. For example, the “hold” task includes various tools like knives, flashlights, cups, and door handles, while a single tool may have multiple affordance labels based on its functions, such as a knife having both “hold” and “clamp”, and a flashlight having both “hold” and “click”. Fig. 6 (b) presents the complex relationships between affordances and object categories using a confusion matrix, highlighting the many-to-many mappings.

Affordance Annotation: For the test set images, we used a heatmap annotation method similar to AGD20K. However, annotators were instructed to emphasize the “functional fingers” contact areas. Three volunteers annotated the interaction regions in the Ego images using the LabelMe tool by drawing polygons around the expected interaction areas based on their “task-tool” usage habits. We averaged the annotations from

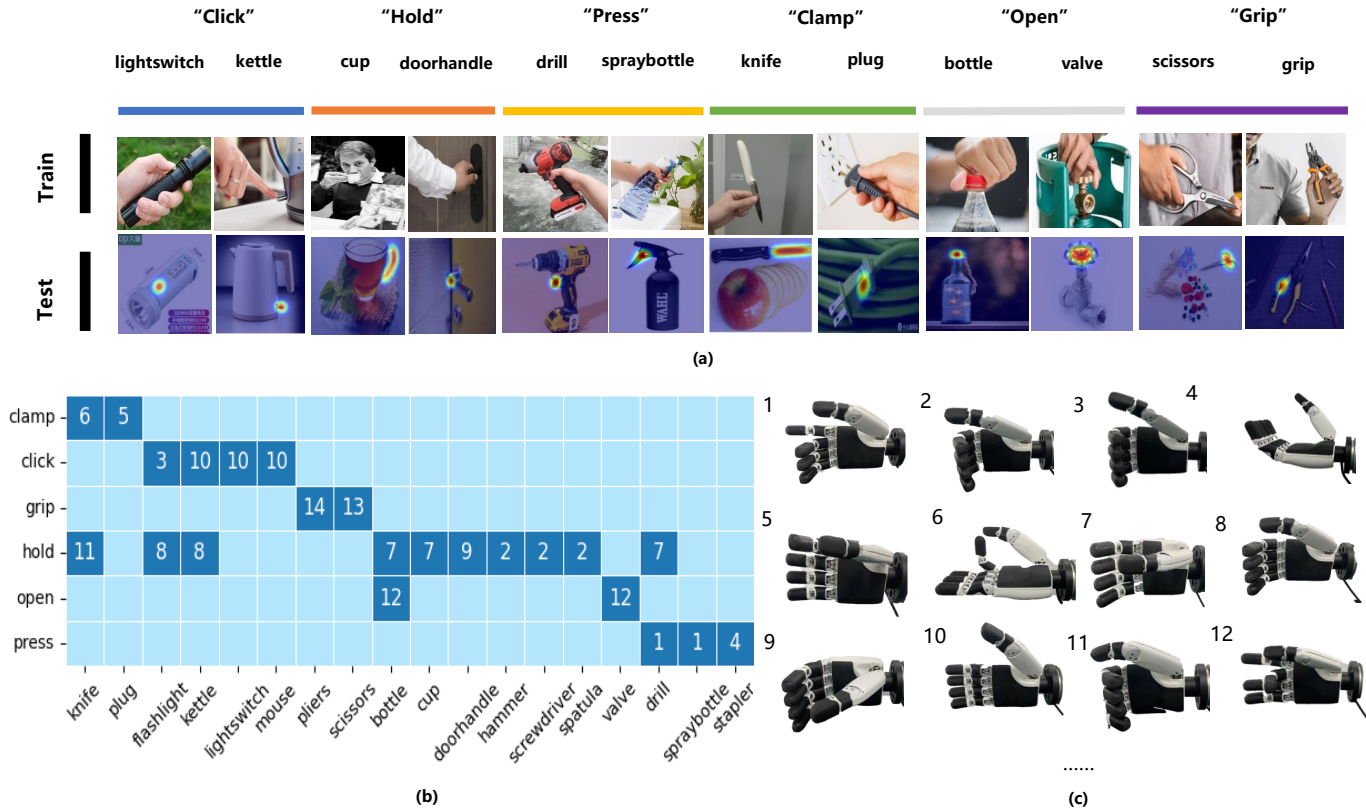


Fig. 6. The properties of the FAH dataset. (a) Some examples from the dataset. (b) Confusion matrix between the affordance category and the object category in FAH, where the horizontal axis denotes the object category and the vertical axis denotes the affordance (task) category, and the numbers in the table represent the corresponding coarse gestures. (c) Examples of categories of coarse gestures.

the three volunteers and applied Gaussian blur to the results. Examples are shown in Fig. 6 (a).

Coarse Gesture Annotation: We annotated a coarse gesture for each “task-tool” combination. Through experimentation, we have identified 14 coarse gestures as shown in Fig. 6 (c) from the 23 mapping relationships. We recorded specific parameters for these 14 gestures, including the flexion angles of the five fingers and the abduction angle of the thumb. It is noteworthy that our method is not specific to any particular robotic hand; different robotic hands can use our method by adjusting the parameters of the 14 coarse grasp gestures accordingly.

VI. EXPERIMENTS

We validate our approach on three levels. First, we perform both qualitative and quantitative evaluations of the affordance localization algorithm based on functional fingers on the dataset. Second, we validate the coarse gesture prediction based on affordances on the dataset. Finally, we conduct real-world dexterous grasping experiments with fixed rotational directions to verify the affordance localization, coarse grasp gesture prediction, and overall functional grasp success rate of our algorithm in practical scenarios. Our demonstration video on the tasks is available at <https://youtu.be/625R26jtwpA>.

A. Setups

Implementation Details. We use the ImageNet [50] pre-trained (without supervision) DINO-ViT-S [47] with a patch size of 16 to generate deep features. In each iteration, N exocentric images along with one egocentric image are taken as input (N is set to 3). Images are first resized to 512×512 and then randomly cropped to 448×448 , followed by random horizontal flipping. SGD with a learning rate of $1e-3$, weight decay of $5e-4$, and a batch size of 3 is used for parameter optimization. Loss weight coefficients λ_c are set to 0.07, and the margin α is set to 0.5. For the first epoch, we warm up the network without L_{cos} , as initial localization maps are not accurate for supervision.

Metrics. For the task of affordance grounding, we employ the commonly used Kullback-Leibler Divergence (KLD), Similarity (SIM), and Normalized Scanpath Saliency (NSS) to evaluate the similarity and correspondence between ground truth and predictions as previous works [24], [25].

For the gesture type prediction task, the precision for each tool j in task t , denoted as $P_{j,t}$, is computed using the formula $P_{j,t} = \frac{\text{TP}_{j,t}}{\text{TP}_{j,t} + \text{FP}_{j,t}}$, where $\text{TP}_{j,t}$ and $\text{FP}_{j,t}$ are the numbers of true positives and false positives, respectively. The average precision, $\text{AP} = \frac{\sum P_{j,t}}{D}$, is calculated where D represents the aggregation level: n_j for the average precision per tool across all tasks, n_t for the average precision per task, or N for the overall success rate, with N being the total number of task-tool

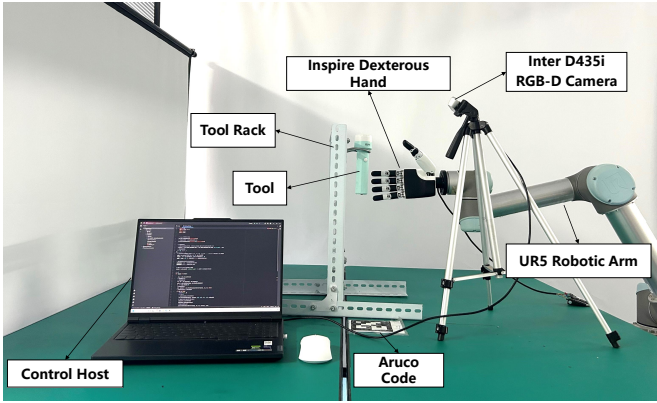


Fig. 7. The real robot platform. In particular, we use Intel D435i cameras, Inspire dexterous hands, and UR5 robotic arms for the experiments.

TABLE II

COMPARISON TO STATE-OF-THE-ART METHODS FROM RELEVANT TASKS ON THE FAH DATASET. THE **BEST** AND **SECOND-BEST** RESULTS ARE HIGHLIGHTED IN BOLD AND UNDERLINED, RESPECTIVELY (\uparrow/\downarrow MEANS HIGHER/LOWER IS BETTER).

Model	KLD (\downarrow)	SIM (\uparrow)	NSS (\uparrow)
Cross-view-AG [25]	1.682	0.271	1.149
LOCATE [24]	<u>1.541</u>	0.33	<u>1.158</u>
Ours	1.459	<u>0.327</u>	1.242

combinations assessed.

For the task of dexterous grasp, we employ the grasp success rate as the metric, as introduced [46]. A successful grasp is defined as the hand maintaining a stable grip on an object for at least ten seconds, and the fingers correctly performing the intended action on the functional area of a tool.

Hardware Setup. For our empirical studies, we constructed a real-world experimental platform depicted in Fig. 7. The platform comprises an Inspire Hand, a UR5 industrial robotic arm, an Intel RealSense D435i camera, a tool holder, and a control computer. The Inspire Hand, a low-cost anthropomorphic manipulator, boasts six degrees of freedom: two for the thumb and one for each of the remaining digits. Actuation for each degree of freedom is provided by a linear motor. A 1-D force sensor and a position sensor are mounted at the end of the drive train to detect force and position in real-time.

B. Results of Functional Affordance Grounding

In this section, we present both qualitative and quantitative results to demonstrate the effectiveness and efficiency of our proposed FunCATE module. Our baselines include Cross-view-AG [25] and LOCATE [24].

Quantitative results. We present the performance of the latest methods from related tasks, which involve weakly supervised object localization. As shown in Tab. II, our method demonstrates significant improvements over competing methods across most metrics. Specifically, our approach achieves a 5.3% improvement in KLD and a 7.3% improvement in NSS over the state-of-the-art grounding method LOCATE [24]. Our SIM score of 0.327 is slightly lower than LOCATE’s score of 0.33. This minor reduction is because SIM focuses more on the similarity of overlapping regions rather than their size.

TABLE III
IMPACT OF VARYING r ON KLD, SIM, AND NSS METRICS. THE **BEST** IS HIGHLIGHTED IN BOLD (\uparrow/\downarrow MEANS HIGHER/LOWER IS BETTER).

r	KLD (\downarrow)	SIM (\uparrow)	NSS (\uparrow)
50	1.501	0.324	1.193
40	1.497	0.324	1.199
30	1.495	0.322	1.205
20	1.459	0.327	1.242
10	1.496	0.324	1.199

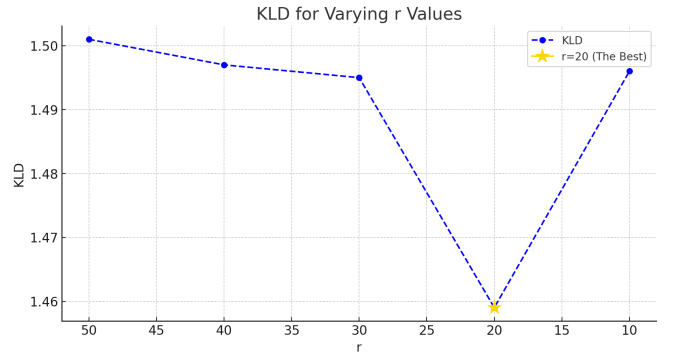


Fig. 8. Line plot of the KLD results for varying r values (Lower is better, and there is no value at the dotted line connection).

While LOCATE also performs part-level detection, it heavily relies on pre-trained DINO-ViT [47] for extracting part-level features, which are then clustered into background, human, and object categories, often neglecting the decoupling of fine-grained, object-related part features. In contrast, our approach, by localizing functional fingers during hand-object interactions, extracts more detailed functional part-level features of objects, enhancing the precision of our localization and facilitating a deeper and more effective transfer of knowledge, leading to superior performance in other metrics.

Qualitative Analysis. We present the visibility grounding visualizations of two baseline methods, our method, and the Ground Truth (GT). As shown in Fig. 9, our visibility localization is more concentrated in the areas where functional fingers should contact, compared to the two baseline methods. We highlighted our method’s predictions with pink dashed boxes, which are essential for dexterous manipulation oriented toward functional usage. When the robot performs the corresponding actions in the “Task Tool” scenarios, stricter functional area localization is required. Particularly for tools like drills and flashlights that have specific buttons, corresponding to the first and third images in the fourth row of Fig. 9, our method accurately localizes to smaller button areas. For tools without buttons, our method also successfully localizes to the areas consistent with the human functional fingers. For instance, in the “Clamp Plug” task, the localization is on the right side of the plug’s head, which is the area the index finger needs to contact. Similarly, in the “Hold Doorhandle” task, the localization is towards the front part of the handle, which is often contacted by the thumb.

Hyperparameter Analysis. We have further investigated the impact of the ROI feature range guided by functional finger

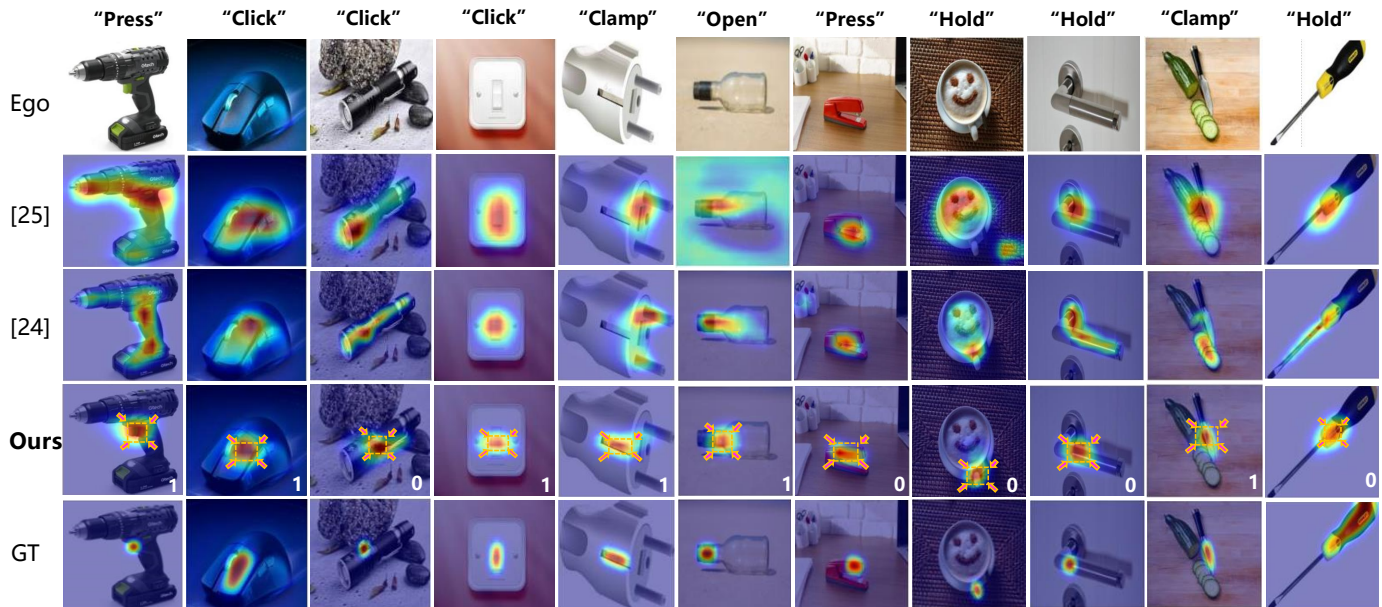


Fig. 9. Qualitative comparison of our method with state-of-the-art functionality grounding methods (LOCATE [24], Cross-view-AG [25]). The numbers “0” and “1” in the fourth row of each image represent the functional finger numbers as calculated by Sec. IV-A2 when performing the task with this object, where 0 denotes the thumb and 1 denotes the index finger. This aids in illustrating that our affordance localization is more concentrated on the regions that the functional fingers should contact, making it more favorable for the functional grasping of tools compared to the other two algorithms.

TABLE IV

PRECISION OF PREDICTED GRASPING GESTURES FOR 6 TASKS AND 18 TOOLS. (FLASHLIGHT: FL, HAMMER: HM, KETTLE: KT, SPATULA: SP, SCISSORS: SC, CUP: CP, DOORHANDLE: DH, BOTTLE: BT, KNIFE: KN, SCREWDRIVER: SD, DRILL: DR, STAPLER: ST, SPRAYBOTTLE: SB, LIGHTSWITCH: LS, MOUSE: MS, PLUG: PG, PLIERS: PL, VALVE: VL, AVERAGE PRECISION: AP)

	FL.	HM.	KT.	SP.	SC.	CP.	DH.	BT.	KN.	SD.	DR.	ST.	SB.	LS.	MS.	PG.	PL.	VL.	AP
Hold	50	100	50	50	25	100	33.33	100	100	100	100	-	-	-	-	-	-	-	73.48
Press	-	-	-	-	-	-	-	-	-	-	100	50	100	-	-	-	-	-	83.33
Click	50	-	50	-	-	-	-	-	-	-	-	-	-	50	100	-	-	-	62.5
Clamp	-	-	-	-	-	-	-	-	100	-	-	-	-	-	-	33.33	-	-	66.67
Grip	-	-	-	-	100	-	-	-	-	-	-	-	-	-	-	-	50	-	75
Open	-	-	-	-	-	-	-	100	-	-	-	-	-	-	-	-	-	100	100
AP	50	100	50	50	62.6	100	33.33	100	100	100	100	50	100	50	100	33.33	50	100	74.65

coordinates. In Fig. 8 and Tab. III, we show the effects of varying $r=\{10, 20, 30, 40, 50\}$ on the metrics KLD, SIM, and NSS. It can be observed that when $r=20$, both KLD, SIM and NSS achieve optimal performance. This is consistent with the principle of our algorithm design: a too-large ROI feature extraction range captures excessive background noise, while a too-small ROI range fails to fully capture the tool button features due to finger occlusion.

Result of Coarse Gesture Predictor

Tab. IV presents the precision of predicted grasping gestures for 6 tasks and 18 tools. The analysis focuses on three main aspects:

Overall Success Rate. The average success rate across all tasks and tools is approximately 74.65%. This indicates that on average, the success rate of predicting the correct grasping gesture for any given task-tool combination is relatively high. The highest success rate is observed in the “Click Mouse”, “Hold cup”, “Hold bottle”, “Open bottle”, and “Grip Scissors” with a rate of 100%, whereas the lowest precision 25% is in “Hold Scissors”.

Average precision per Task. Our method achieves high average precision across six tasks with various tools. The highest is for the task “Open”, with an average precision of 100%, while the lowest is for “Click”, with a precision of 62.5%. Notably, even for the task “Hold”, which involves eleven different types of operating tools, the method maintains an average precision of 73.48%. This demonstrates our method’s ability to extract common features across different objects in learning dexterous manipulations.

Success Rate per Tool. The success rate exhibits significant variability across different tools. Tools such as “Cup”, “Bottle”, and “Screwdriver” achieve a prediction success rate of 100%. Conversely, tools like “Doorhandle” and “Plug” demonstrate a much lower precision rate of only 33.33%. We hypothesize that this reduced accuracy is due to the more subtle and less distinctive interaction features present in the areas of hand-tool interaction for these tools. The lack of prominent characteristics makes it challenging for our gesture prediction module, which relies on discerning these features, to accurately predict the correct manipulative actions.

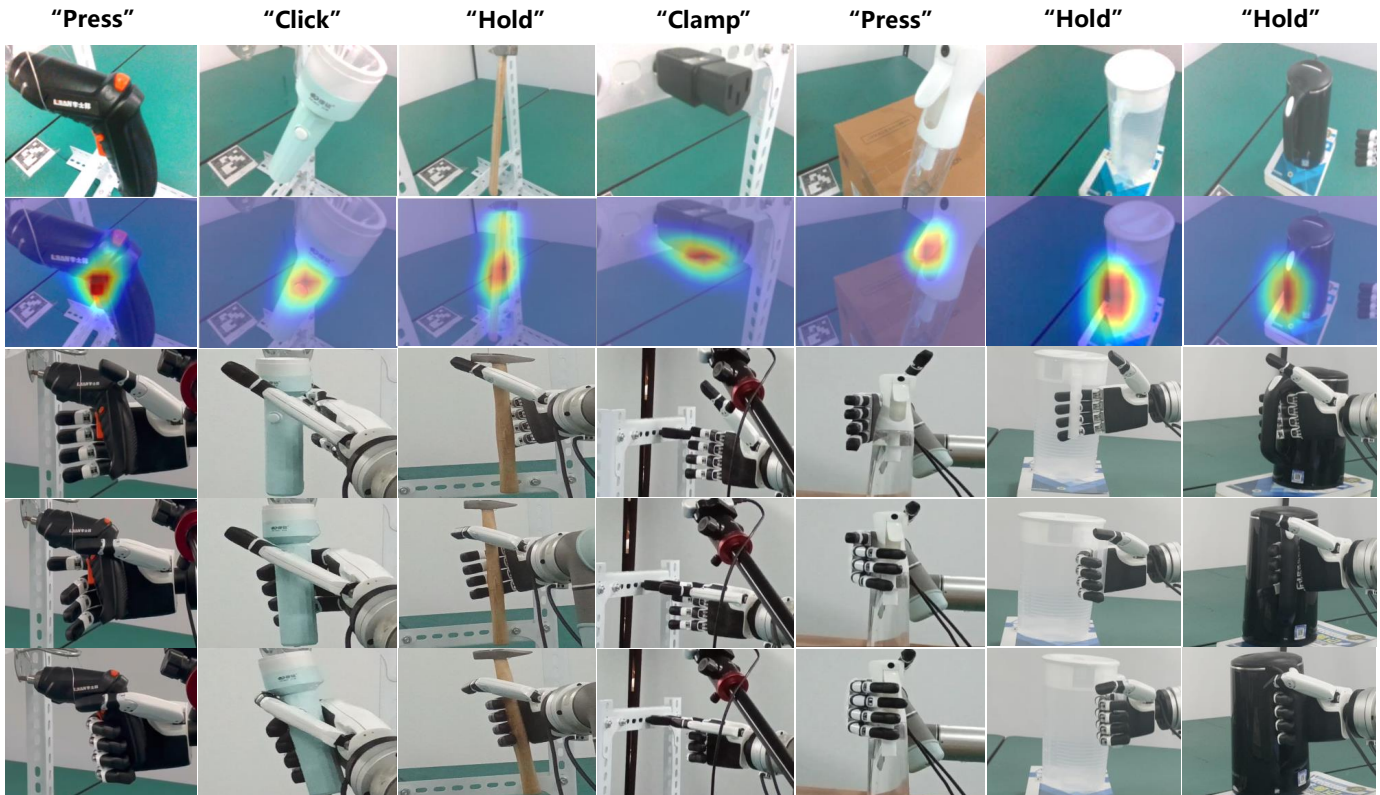


Fig. 10. Examples of dexterous grasping based on our granularity-aware affordance understanding algorithm; Row 1 - Ego image from camera view; Row 2 - Functional-finger-guided fine-grained affordance localization visualization; Row 3 - Approaching based on localization; Row 4 - Coarse grasping executed by affordance-driven mechanical gesture prediction network; Row 5 - Fine grasping adjustment based on force feedback.

C. Performance on Daily Real Objects

We have conducted experimental verification on tool instances not included in the training set within real-world scenarios. Firstly, we demonstrated the precise localization and gesture understanding capabilities of our method across different *task-tool* combinations. Subsequently, we showcased the steps of functional grasping completed by our method, including overall localization, coarse gesture prediction, and fine-grained grasping. Finally, we quantitatively analyzed the success rates of localization, coarse gesture prediction, and functional grasping for several commonly used tools over 15 experiments in real-world scenarios. Although our dataset does not include laboratory scenarios and the specific tools used in our experiments, our method still performed well in unseen scenarios and similar unseen objects.

Firstly, our algorithm provides different region localizations and grasping gestures based on the task. Fig. 11 (a) depicts the task of “Press Drill”, where the proposed solution accurately localizes the button area and provides a coarse grasping gesture “type1” that aligns with human grasping habits. Fig. 11 (c) shows the task of “Hold Drill”, where our method localizes the handle area and provides a “type2” grasping gesture. For the same task, our algorithm also provides different region localizations and grasping gestures based on the tool. As shown in Fig. 11 (b), the second row depicts the task of “Press Stapler”. Our method localizes the head area of the stapler and provides a “type3” grasping gesture. This is distinct from the

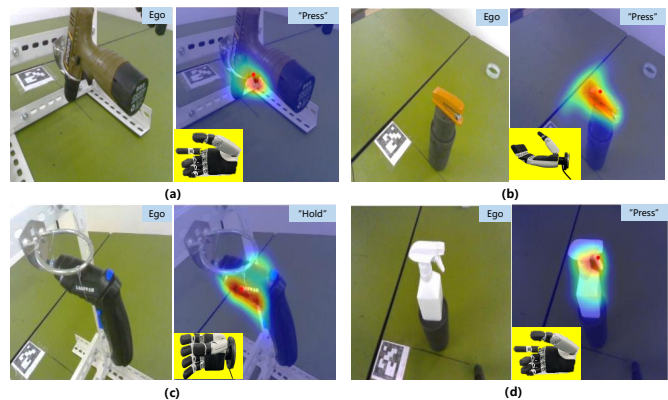


Fig. 11. Examples of functional affordance positioning and coarse gesture prediction ability in real scenarios.

localization and gesture provided for the “Press Drill” task, even though both tasks are “Press”. Additionally, our model exhibits the ability to generalize task understanding for tools with similar usage habits. For instance, comparing Fig. 11 (a) and Fig. 11 (d), both “Press Drill” and “Press Spray Bottle” tasks localize the button area and provide a “type2” grasping gesture. This is due to the similar structure and usage of the drill and the spray bottle.

Secondly, as shown in Fig. 10, the second row displays the visualizations of our functional affordance localization. For tasks sensitive to finger positioning such as “Press Drill”,

TABLE V

THE SUCCESS RATE OF THE REPRESENTATIVE “*Task Tool*” ACROSS 15 TRIALS IN REAL-WORLD EXPERIMENTS. (POSITIONING SUCCESS RATE: Pos., COARSE GESTURE PREDICTION SUCCESS RATE: CG., FUNCTIONAL GRASP SUCCESS RATE: FG.)

	Press DR.	Hold DR.	Hold KT.	Click FL.	Hold HM.	Press SB.
Pos.	66.67	13.33	86.67	66.67	93.33	93.33
CG.	46.67	93.33	100	66.67	93.33	46.67
FG.	26.67	40	86.67	66.67	73.33	46.67



Fig. 12. The presentation of failure cases. The green circle represents the area that should be located.

“*Click Flashlight*”, and “*Press Spraybottle*”, our method accurately localizes the buttons on the drill, flashlight switch, and spray bottle button, as illustrated in the first three columns of the second row, consistent with the design intent of our finger-guided affordance localization network. For tasks like “*Hold Hammer*” and “*Hold Kettle*”, which are less sensitive to finger positioning, our method still accurately localizes the corresponding handle positions, as shown in the last three columns of the second row. The third row of Fig. 10 demonstrates the effects of our model-based finger-end transformation module, enabling the robotic arm to accurately move to the grasping point. The fourth row shows the execution results of our coarse affordance gesture prediction module. The fifth row illustrates the final stable functional grasping results after angle adjustments based on the coarse gestures. For the “*Press Drill*” and “*Press Spraybottle*” tasks, the index finger accurately presses the button while the remaining fingers firmly grasp the handle. In the “*Click Flashlight*” task, the thumb precisely presses the switch while the other fingers grip the handle. This demonstrates the contribution of each module to functional grasping. In summary, our approach enables stable functional grasping by first performing functional localization and coarse gesture prediction, followed by angle refinement.

Finally, we recorded the success rates of localization, coarse gesture prediction, and functional grasping for several representative “*Task-Tool*” across 15 times in real-world experiments. As shown in Tab. V, except for “*Hold Drill*”, all other localization success rates exceeded 50%. Specifically, the success rates for the hammer handle and kettle handle, which have larger localization areas, were as high as 93.33% and 86.67%, respectively. The localization success rate for “*Hold Drill*” was only 13%, which is attributed to the used backbone model DINO-VIT [47]. This model, which provides

part-level features, struggles with effectively extracting features from the drill head, which does not belong to part-level characteristics. When examining the success rates of coarse gesture prediction, we found that *Hold* tasks had high success rates, above 93.33%, while other tasks were relatively lower. Finally, regarding the success rates of functional grasping, we observed that despite occasional errors in localization or coarse gesture prediction, functional grasping could still be achieved. For instance, although the localization success rate for “*Hold Drill*” was only 13.33%, the grasping task could still be completed because accurate localization was less critical for grasping the drill. Even when the localization was slightly above the button, successful grasping was still possible. Conversely, for “*Task-tool*” with high localization and coarse gesture prediction success rates, we occasionally observed lower functional grasping success rates. For example, the “*Press Drill*” task requires precise pressing of the button with the functional finger, posing a significant challenge for the end-effector grasping point selection. Although our model-based coordinate transformation method achieved some success, the presence of error propagation prevented precise localization. This indicates an area for further improvement.

VII. DISCUSSION

Fig. 12 illustrates some failure cases of the functional affordance localization module in both the dataset (first row) and real-world scenarios (second row). For the “*Grip Scissors*” task, our method incorrectly localized at the junction of the handle and scissors instead of within the circle of the scissors. Similarly, for the “*Open Valve*” task, the localization was erroneously placed slightly below the valve. We attribute these errors to the fact that the features of the functional fingers selected during training coincided with those regions.

Although our method can effectively locate more fine-grained tool areas, depth extraction in real scenes is extremely sensitive due to the difficulty of positioning in a smaller range. In the future, we will devote ourselves to the localization research of 3D scenes. At the same time, we do not consider the rotation quantity of grasp, and we will devote ourselves to the research of rotation quantity of affordance in the future. Finally, in complex scenes where there are multiple objects and we cannot correctly select a single object, we will continue to consider this challenging task.

VIII. CONCLUSION

In this work, we propose a weakly supervised method to learn affordance cues from exocentric images of hand-object interactions. These cues are used to supervise the corresponding features in Ego images containing only objects. This enables the localization of functional grasping areas and coarse grasp gestures during the testing phase. Additionally, we design a model-based post-processing module that refines the localized regions and coarse grasp gestures to determine the wrist-end grasp points and adjust the grasp from coarse to fine, ultimately satisfying functional grasping conditions. We created a small-scale dataset of hand-object interactions

relevant to functional grasping to train our method. Extensive real-world experiments demonstrate that our approach significantly outperforms state-of-the-art methods, achieving more focused and precise localization, providing dexterous coarse gestures for different tasks, and successfully performing functional grasps based on these foundations.

REFERENCES

- [1] Y. Zhang *et al.*, “FunctionalGrasp: Learning functional grasp for robots via semantic hand-object representation,” *IEEE Robotics and Automation Letters*, vol. 8, no. 5, pp. 3094–3101, 2023.
- [2] M. Kovic, D. Kragic, and J. Bohg, “Learning task-oriented grasping from human activity datasets,” *IEEE Robotics and Automation Letters*, vol. 5, no. 2, pp. 3352–3359, 2020.
- [3] Y. Xiang, T. Schmidt, V. Narayanan, and D. Fox, “PoseCNN: A convolutional neural network for 6D object pose estimation in cluttered scenes,” in *Proc. RSS*, 2018.
- [4] S. Yu, D. Zhai, Y. Guan, and Y. Xia, “Category-level 6-D object pose estimation with shape deformation for robotic grasp detection,” *IEEE Transactions on Neural Networks and Learning Systems*, 2023.
- [5] E. Corona, A. Pumarola, G. Alenyà, F. Moreno-Noguer, and G. Rogez, “GanHand: Predicting human grasp affordances in multi-object scenes,” in *Proc. CVPR*, 2020, pp. 5030–5040.
- [6] J. Jian, X. Liu, M. Li, R. Hu, and J. Liu, “AffordPose: A large-scale dataset of hand-object interactions with affordance-driven hand pose,” in *Proc. ICCV*, 2023, pp. 14 667–14 678.
- [7] L. Yang *et al.*, “OakInk: A large-scale knowledge repository for understanding hand-object interaction,” in *Proc. CVPR*, 2022, pp. 20 921–20 930.
- [8] P. Mandikal and K. Grauman, “Learning dexterous grasping with object-centric visual affordances,” in *Proc. ICRA*, 2021, pp. 6169–6176.
- [9] H. Jiang, S. Liu, J. Wang, and X. Wang, “Hand-object contact consistency reasoning for human grasps generation,” in *Proc. ICCV*, 2021, pp. 11 087–11 096.
- [10] B. Wu *et al.*, “Generative attention learning: A “general” framework for high-performance multi-fingered grasping in clutter,” *Autonomous Robots*, vol. 44, no. 6, pp. 971–990, 2020.
- [11] H. Li, Y. Zhang, Y. Li, and H. He, “Learning task-oriented dexterous grasping from human knowledge,” in *Proc. ICRA*, 2021, pp. 6192–6198.
- [12] J. J. Gibson, “The theory of affordances,” *Hilldale, USA*, vol. 1, no. 2, pp. 67–82, 1977.
- [13] R. Xu, F.-J. Chu, C. Tang, W. Liu, and P. A. Vela, “An affordance keypoint detection network for robot manipulation,” *IEEE Robotics and Automation Letters*, vol. 6, no. 2, pp. 2870–2877, 2021.
- [14] M. Stark, P. Lies, M. Zillich, J. Wyatt, and B. Schiele, “Functional object class detection based on learned affordance cues,” in *Proc. ICVS*, 2008, pp. 435–444.
- [15] H. Kjellström, J. Romero, and D. Kragić, “Visual object-action recognition: Inferring object affordances from human demonstration,” *Computer Vision and Image Understanding*, vol. 115, no. 1, pp. 81–90, 2011.
- [16] T. Nagarajan, C. Feichtenhofer, and K. Grauman, “Grounded human-object interaction hotspots from video,” in *Proc. ICCV*, 2019, pp. 8687–8696.
- [17] J. Chen, D. Gao, K. Q. Lin, and M. Z. Shou, “Affordance grounding from demonstration video to target image,” in *Proc. CVPR*, 2023, pp. 6799–6808.
- [18] H. Luo, W. Zhai, J. Zhang, Y. Cao, and D. Tao, “Learning visual affordance grounding from demonstration videos,” *IEEE Transactions on Neural Networks and Learning Systems*, 2023.
- [19] D. F. Fouhey, X. Wang, and A. Gupta, “In defense of the direct perception of affordances,” *arXiv preprint arXiv:1505.01085*, 2015.
- [20] J. Mi, S. Tang, Z. Deng, M. Goerner, and J. Zhang, “Object affordance based multimodal fusion for natural human-robot interaction,” *Cognitive Systems Research*, vol. 54, pp. 128–137, 2019.
- [21] J. Mi *et al.*, “Intention-related natural language grounding via object affordance detection and intention semantic extraction,” *Frontiers in Neurorobotics*, vol. 14, p. 26, 2020.
- [22] H. Luo, W. Zhai, J. Zhang, Y. Cao, and D. Tao, “Learning visual affordance grounding from demonstration videos,” *IEEE Transactions on Neural Networks and Learning Systems*, 2023.
- [23] Y. Li, T. Nagarajan, B. Xiong, and K. Grauman, “Ego-Exo: Transferring visual representations from third-person to first-person videos,” in *Proc. CVPR*, 2021, pp. 6943–6953.
- [24] G. Li, V. Jampani, D. Sun, and L. Sevilla-Lara, “LOCATE: Localize and transfer object parts for weakly supervised affordance grounding,” in *Proc. CVPR*, 2023, pp. 10 922–10 931.
- [25] H. Luo, W. Zhai, J. Zhang, Y. Cao, and D. Tao, “Learning affordance grounding from exocentric images,” in *Proc. CVPR*, 2022, pp. 2242–2251.
- [26] T. Feix, J. Romero, H.-B. Schmiemayer, A. M. Dollar, and D. Kragic, “The grasp taxonomy of human grasp types,” *IEEE Transactions on Human-Machine Systems*, vol. 46, no. 1, pp. 66–77, 2016.
- [27] H. Luo, W. Zhai, J. Zhang, Y. Cao, and D. Tao, “Grounded affordance from exocentric view,” *International Journal of Computer Vision*, vol. 132, no. 6, pp. 1945–1969, 2024.
- [28] X. Zhan *et al.*, “OAKINK2: A dataset of bimanual hands-object manipulation in complex task completion,” in *Proc. CVPR*, 2024, pp. 445–456.
- [29] H. Luo, W. Zhai, J. Zhang, Y. Cao, and D. Tao, “One-shot affordance detection,” *arXiv preprint arXiv:2106.14747*, 2021.
- [30] Y. Hasson *et al.*, “Learning joint reconstruction of hands and manipulated objects,” in *Proc. CVPR*, 2019, pp. 11 807–11 816.
- [31] F.-J. Chu, R. Xu, and P. A. Vela, “Learning affordance segmentation for real-world robotic manipulation via synthetic images,” *IEEE Robotics and Automation Letters*, vol. 4, no. 2, pp. 1140–1147, 2019.
- [32] P. Ardón, È. Pairet, R. P. A. Petrick, S. Ramamoorthy, and K. S. Lohan, “Learning grasp affordance reasoning through semantic relations,” *IEEE Robotics and Automation Letters*, vol. 4, no. 4, pp. 4571–4578, 2019.
- [33] W. Chen, H. Liang, Z. Chen, F. Sun, and J. Zhang, “Learning 6-DoF task-oriented grasp detection via implicit estimation and visual affordance,” in *Proc. IROS*, 2022, pp. 762–769.
- [34] Y. Song, P. Sun, Y. Ren, Y. Zheng, and Y. Zhang, “Learning 6-DoF fine-grained grasp detection based on part affordance grounding,” *arXiv preprint arXiv:2301.11564*, 2023.
- [35] T. Nguyen *et al.*, “Language-conditioned affordance-pose detection in 3D point clouds,” *arXiv preprint arXiv:2309.10911*, 2023.
- [36] H. Luo, W. Zhai, J. Zhang, Y. Cao, and D. Tao, “Leverage interactive affinity for affordance learning,” in *Proc. CVPR*, 2023, pp. 6809–6819.
- [37] C.-Y. Chuang, J. Li, A. Torralba, and S. Fidler, “Learning to act properly: Predicting and explaining affordances from images,” in *Proc. CVPR*, 2018, pp. 975–983.
- [38] A. Rodriguez, M. T. Mason, and S. Ferry, “From caging to grasping,” *The International Journal of Robotics Research*, vol. 31, no. 7, pp. 886–900, 2012.
- [39] C. Rosales, R. Suárez, M. Gabiccini, and A. Bicchi, “On the synthesis of feasible and prehensile robotic grasps,” in *Proc. ICRA*, 2012, pp. 550–556.
- [40] S. El-Khoury, R. De Souza, and A. Billard, “On computing task-oriented grasps,” *Robotics and Autonomous Systems*, vol. 66, pp. 145–158, 2015.
- [41] R. M. Murray, Z. Li, and S. S. Sastry, *A mathematical introduction to robotic manipulation*. CRC press, 2017.
- [42] W. Shang, F. Song, Z. Zhao, H. Gao, S. Cong, and Z. Li, “Deep learning method for grasping novel objects using dexterous hands,” *IEEE Transactions on Cybernetics*, vol. 52, no. 5, pp. 2750–2762, 2022.
- [43] V. Mayer, Q. Feng, J. Deng, Y. Shi, Z. Chen, and A. Knoll, “FFHNet: Generating multi-fingered robotic grasps for unknown objects in real-time,” in *Proc. ICRA*, 2022, pp. 762–769.
- [44] W. Wei *et al.*, “DVG: Deep variational grasp generation for dextrous manipulation,” *IEEE Robotics and Automation Letters*, vol. 7, no. 2, pp. 1659–1666, 2022.
- [45] H. Wang, H. Zhang, L. Li, Z. Kan, and Y. Song, “Task-driven reinforcement learning with action primitives for long-horizon manipulation skills,” *IEEE Transactions on Cybernetics*, 2023.
- [46] T. Zhu, R. Wu, J. Hang, X. Lin, and Y. Sun, “Toward human-like grasp: Functional grasp by dexterous robotic hand via object-hand semantic representation,” *IEEE Transactions on Pattern Analysis and Machine Intelligence*, vol. 45, no. 10, pp. 12 521–12 534, 2023.
- [47] M. Caron *et al.*, “Emerging properties in self-supervised vision transformers,” in *Proc. ICCV*, 2021, pp. 9630–9640.
- [48] C. Liguori *et al.*, “MediaPipe: A framework for building perception pipelines,” *arXiv preprint arXiv:1906.08172*, 2019.
- [49] B. Zhou, A. Khosla, A. Lapedriza, A. Oliva, and A. Torralba, “Learning deep features for discriminative localization,” in *Proc. CVPR*, 2016, pp. 2921–2929.
- [50] J. Deng, W. Dong, R. Socher, L.-J. Li, K. Li, and L. Fei-Fei, “ImageNet: A large-scale hierarchical image database,” in *Proc. CVPR*, 2009, pp. 248–255.